symmetry

MDPI

Article

Deployment and Retrieval Missions from Quasi-Periodic and Chaotic States under a Non-Linear Control Law

Francisco J. T. Salazar [1,*] and Antonio B. A. Prado [1,2]

[1] National Institute for Space Research, Av. dos Astronautas-Campus do CTA, São José dos Campos 12227-010, SP, Brazil; antonio.prado@inpe.br
[2] Academy of Engineering, Peoples' Friendship University of Russia (RUDN University), 6 Miklukho-Maklaya Street, 117198 Moscow, Russia
* Correspondence: e7940@hotmail.com; Tel.: +55-12-981015572

Abstract: When the length of the tether remains constant, the relative planar motion of the tethered subsatellite with respect to the base satellite in a circular orbit around the Earth, is similar to a simple pendulum motion, i.e., there are two kinds of equilibrium points: local vertical and local horizontal positions, which are center and saddle points, respectively. However, when out-of-plane motion is initially excited, the relative motion of the subsatellite presents symmetric quasi-periodic and chaotic behavior. In the first part of this study, such trajectories are analyzed by means of Poincaré sections. In the second part, a non-linear tension force by using a Lyapunov approach is proposed for controlling the coupled pitch-roll motion during the deployment and retrieval phases. The goal of this paper is to guide the relative non-linear motion of the subsatellite to the local upward vertical position. The numerical results show that the non-linear tension control steered the subsatellite close to the local vertical direction very well, reducing the quasi-periodic and chaotic oscillations.

Keywords: tethered satellite system; quasi-periodic and chaotic motions; lyapunov approach; tension control law

Citation: Salazar, F.J.T.; Prado, A.B.A. Deployment and Retrieval Missions from Quasi-Periodic and Chaotic States under a Non-Linear Control Law. *Symmetry* **2022**, *14*, 1381. https://doi.org/10.3390/sym14071381

Academic Editor: Jan Awrejcewicz

Received: 6 May 2022
Accepted: 4 July 2022
Published: 5 July 2022

1. Introduction

In recent decades, the Tethered Satellite System (TSS) has been proposed for many different space applications, such as micro- and variable-g experiments, orbit transfer, spacecraft formation, energy transmission, and space debris removal [1]. However, one of the primary issues in space tether missions is controlling the fast deployment and retrieval of attached payloads, which is extremely complicated due to nonlinear dynamics. Furthermore, chaotic motion can occur in a two-body TSS [2–15]. The Coriolis force causes the deployment/retrieval operation to be unstable. In fact, the retrieval operation is inherently unstable [3,16,17]. Many researchers have investigated the dynamics and control of a TSS during deployment, station-keeping, and retrieval stages, and various methods for controlling tether deployment/retrieval have been proposed, such as tension control laws, length rate control algorithms, Lyapunov's second method, optimal control strategies, elastic tethers, and out-of-plane thrusting [3,15,18–39].

Because of the complexity of the problem, a TSS consisting of a base satellite and a subsatellite linked by a rigid but massless tether, orbiting the Earth in a Keplerian circular orbit, was considered in this study. Other forces or perturbations were neglected. Additionally, the base satellite was regarded as the reference spacecraft, and its mass was assumed to be much greater than that of the subsatellite. In such cases, Misra et al. [6] showed that, in the station-keeping phase, the planar motion of the tethered subsatellite had two kinds of equilibrium points–center and saddle points–at the local vertical and local horizontal positions, respectively. Thus, its planar motion when the tether length was constant did not seem to be quite complicated. However, during deployment and retrieval, the subsatellite did not move in a straight line trajectory because of the Coriolis

force [3,16,17,19]. For deployment and retrieval, the dynamics of the tethered subsatellite may become unstable around the local vertical configuration. In fact, if the tether length varies too fast, there will be no fixed points [3]. Therefore, it was necessary to implement a control scheme for the deployment and retrieval phases. In this connection, innumerable control strategies have been studied for the in-plane pitch motion [19,20,23–26,28,29,31,38]. Among these, the tension feedback control laws, as well as the length rate schemes, have been proven to be the most effective for their simplicity and practicality [40].

Under the above assumptions for the dynamics of the station-keeping phase, Misra et al. [6] found that the coupled pitch-roll motion of a TSS will be periodic, quasi-periodic, or chaotic. Misra et al. [6] showed symmetric phase portraits and Poincaré sections of periodic, quasi-periodic, and chaotic motions. Thus, three-dimensional deployment and retrieval missions need further study and numerical experiments. For example, assuming that the base satellite follows a circular orbit, Fujii et al. [24], Vadali and Kim [26], Fujii and Anazawa [27] used the Lyapunov approach to propose two different nonlinear feedback control laws for the deployment and retrieval of a subsatellite swinging in-plane and out-of-plane. Misra and Modi [41] and Nixon [3] studied the coupled motion of deployment and retrieval under a length-rate control algorithm in a circular orbit. Kumar and Pradeep [30], Salazar and Prado [39] linearized the motion equations about the local vertical to derive linear feedback control laws for the three-dimensional dynamics from a circular orbit. In this case, Kumar and Pradeep [30] employed a combination of tension control and out-of-plane thrusting. On the other hand, Salazar and Prado [39] only applied a linear tension control. Finally, Jin and Hu [34] and Wen et al. [35,36] presented a nonlinear optimal control for the deployment and retrieval of a tethered subsatellite system in a circular Keplerian orbit, taking into account not only the in-plane but also the out-of-plane motion. Similarly, the linear tension feedback control laws and the tether rate control laws are easier to implement [40]. However, stability could not be global since these schemes use linear approximations to determine the stability of the fixed points [42]. In this sense, nonlinear feedback control laws, designed using Lyapunov functions (named mission functions), showed excellent controlled response of the tethered subsatellite system because linear approximations were not employed. A positive-definite Lyapunov function is defined to be zero when the deployment and retrieval are essentially completed. A nonlinear tension control is then selected to reduce the value of the Lyapunov function during deployment and retrieval.

The goal of this paper is to analyze the efficiency of a nonlinear tension-control law designed from a Lyapunov function and apply it to deployment and retrieval missions when the initial state emerges from the three-dimensional quasi-periodic and chaotic zones of the TSS dynamics. Lyapunov's second method has been used to select a stable tension-control law during deployment and retrieval in the three-dimensional case, such that the quasi-periodic and chaotic motions are suppressed, and the system is steered close to the local vertical direction. Although much in the literature have been published on the control of deployment and retrieval missions of a TSS, the control of the chaotic behavior observed in the coupled pitch-roll motion has not been sufficiently explored. In this sense, the simulations performed in this study show that the selected nonlinear tension-control law performs well, but terminal oscillations of the rolling motion are encountered during retrieval because this process is inherently unstable, as mentioned above. Additionally, it is important to mention that it is possible to experience quasi-periodic and chaotic planar motions on the TSS when additional forces and perturbations are considered in the motion of TSS around the Earth [6–8,10,15,43]. Although the mathematical model used in this study is simpler than more elaborated in-plane models, the numerical results showed excellent controlled behavior of the nonlinear tension-control law, even for chaotic behavior.

The remainder of this article is as follows. A simplified mathematical model for an orbiting TSS in a Keplerian circular orbit is given in Section 2. Then, the regular and chaotic dynamics in three-dimensional space is analyzed using phase portraits and Poincaré sections in Section 2.1. Section 2.2 describes the mission function, the tension control law,

and its stability. Section 3 provides a case study to verify the quasi-periodic and chaotic motions and their deployment and retrieval performance. Section 4 gives the conclusions.

2. Methods

Figure 1 illustrates a TSS orbiting the Earth in a Keplerian circular orbit. It consists of a base satellite of mass M, which is regarded as the reference spacecraft, and a subsatellite of mass m ($m << M$) connected by a massless and rigid tether. The true anomaly, orbital angular velocity vector, and orbital radius vector from the Earth's center $\boldsymbol{O}$ of the base satellite's orbit are denoted by υ, $\boldsymbol{\omega}$, and $\boldsymbol{R_B}$, respectively, as shown in Figure 1a. Similarly, the reference coordinate system is designated by $\boldsymbol{x_0}$-$\boldsymbol{y_0}$-$\boldsymbol{z_0}$ axes, such that $\boldsymbol{y_0} = \boldsymbol{R_B}/R_B$, and $\boldsymbol{z_0} = \boldsymbol{\omega}/\omega$, as shown in Figure 1.

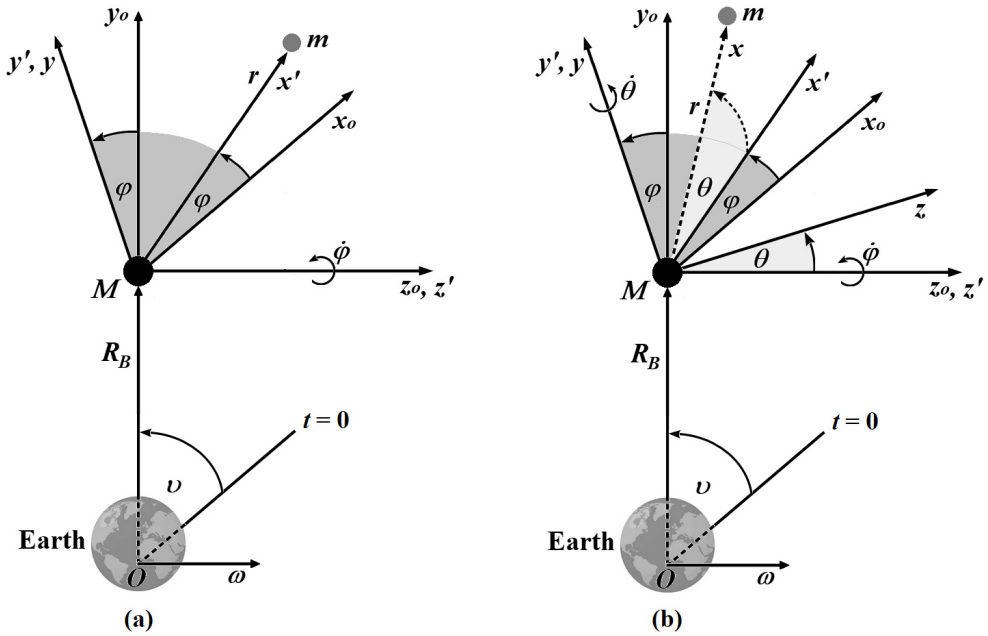

Figure 1. Sketch of the geometry of the TSS around the Earth showing reference coordinate systems and the spherical coordinate system. (**a**) Pitch motion is obtained by rotating $\boldsymbol{x_0}$-$\boldsymbol{y_0}$ axes through an angle φ. (**b**) Roll motion is obtained by rotating $\boldsymbol{x'}$-$\boldsymbol{z'}$ axes through an angle θ [39].

The relative motion of the subsatellite is represented by the radius vector $\boldsymbol{r}$, which is described by its magnitude r, where $r << R_B$, and the pitch and roll angles φ and θ, respectively, as shown in Figure 1a,b. The radius vector motion is described by

$$\ddot{\boldsymbol{r}} = \left(-\frac{\mu}{R_S^3}\boldsymbol{R_S} - \frac{\mathcal{T}}{m}\frac{\boldsymbol{r}}{r}\right) - \left(-\frac{\mu}{R_B^3}\boldsymbol{R_B} + \frac{\mathcal{T}}{M}\frac{\boldsymbol{r}}{r}\right), \tag{1}$$

where μ = 398,602 km^3/s^2 is the Earth's gravitational constant, $\mathcal{T}$ is the magnitude of the tension tether force, $\boldsymbol{R_S} = \boldsymbol{R_B} + \boldsymbol{r}$ is the vector position of the subsatellite from the Earth's center $\boldsymbol{O}$, and overdot denotes the time derivative d/dt. On the fact that $m << M$ and $r << R_B$, $\ddot{\boldsymbol{r}}$ can be estimated as

$$\ddot{\boldsymbol{r}} = -\frac{\mu}{R_B^3}\left[1 - 3\frac{\sin\varphi\cos\theta}{R_B}r\right]\boldsymbol{R_S} + \frac{\mu}{R_B^3}\boldsymbol{R_B} - \frac{\mathcal{T}}{m}\frac{\boldsymbol{r}}{r}. \tag{2}$$

On the other hand, the relative position vector $\boldsymbol{r}$ and the position vector $\boldsymbol{R_B}$ can be expressed in the spherical coordinate system $\hat{\boldsymbol{r}} - \hat{\boldsymbol{\varphi}} - \hat{\boldsymbol{\theta}}$ as [31]

$$\boldsymbol{r} = r\hat{\boldsymbol{r}}, \quad \boldsymbol{R_B} = \cos\theta\sin\varphi\hat{\boldsymbol{r}} + \cos\varphi\hat{\boldsymbol{\varphi}} + \sin\theta\sin\varphi\hat{\boldsymbol{\theta}}. \tag{3}$$

Similarly, the radius vector motion $\ddot{\boldsymbol{r}}$ along $\hat{\boldsymbol{r}} - \hat{\boldsymbol{\varphi}} - \hat{\boldsymbol{\theta}}$ is

$$\ddot{\boldsymbol{r}} = \ddot{r}_r \hat{\boldsymbol{r}} + \ddot{r}_\varphi \hat{\boldsymbol{\varphi}} + \ddot{r}_\theta \hat{\boldsymbol{\theta}}, \tag{4}$$

where

$$\ddot{r}_r = \ddot{r} - r\dot{\theta}^2 - r(\omega + \dot{\varphi})^2 \cos^2\theta, \tag{5}$$
$$\ddot{r}_\varphi = \left[r\ddot{\varphi} + 2\dot{r}(\omega + \dot{\varphi}) - 2r(\omega + \dot{\varphi})\dot{\theta}\tan\theta\right]\cos\theta, \tag{6}$$
$$\ddot{r}_\theta = -\left[r\ddot{\theta} + 2\dot{r}\dot{\theta} + r\left(\omega + \dot{\theta}\right)^2 \cos\theta\sin\theta\right]. \tag{7}$$

Assuming a rigid tether of length ℓ in the TSS, then $\ell = r$. Thus, substituting the spherical coordinates of $\boldsymbol{r}$, $\boldsymbol{R_B}$, and $\ddot{\boldsymbol{r}}$ in Equation (2), the relative motion of the tethered subsatellite is described by the following equations [31]:

$$\ddot{\ell} - \ell\dot{\theta}^2 - \ell(\omega + \dot{\varphi})^2\cos^2\theta - \ell\omega^2\left(3\sin^2\varphi\cos^2\theta - 1\right) = -\frac{\mathcal{T}}{m}, \tag{8}$$
$$\ddot{\varphi} + 2\frac{\dot{\ell}}{\ell}(\omega + \dot{\varphi}) - 2(\omega + \dot{\varphi})\dot{\theta}\tan\theta - 3\omega^2\sin\varphi\cos\varphi = 0, \tag{9}$$
$$\ddot{\theta} + 2\frac{\dot{\ell}}{\ell}\dot{\theta} + (\omega + \dot{\varphi})^2\cos\theta\sin\theta + 3\omega^2\sin^2\varphi\sin\theta\cos\theta = 0. \tag{10}$$

Using the following non-dimensional variables:

$$v = \omega t, \quad \rho = \frac{\ell}{L}, \quad u = \frac{\mathcal{T}}{m\omega^2 L},$$

where L is the maximum tether length, the equations of motion of the subsatellite can be non-dimensionalized:

$$\rho'' - \rho\theta'^2 - \rho\left(1 + \varphi'\right)^2\cos^2\theta - \rho\left(3\sin^2\varphi\cos^2\theta - 1\right) = -u, \tag{11}$$
$$\varphi'' + 2\frac{\rho'}{\rho}\left(1 + \varphi'\right) - 2\left(1 + \varphi'\right)\theta'\tan\theta - 3\sin\varphi\cos\varphi = 0, \tag{12}$$
$$\theta'' + 2\frac{\rho'}{\rho}\theta' + \left(1 + \varphi'\right)^2\cos\theta\sin\theta + 3\sin^2\varphi\sin\theta\cos\theta = 0, \tag{13}$$

where prime refers to the true anomaly derivative $\mathrm{d}/\mathrm{d}v$.

In the station-keeping phase we have $\ell' = 0$. Then Equations (11)–(13) reduce to

$$\varphi'' - 2\left(1 + \varphi'\right)\theta'\tan\theta - 3\sin\varphi\cos\varphi = 0, \tag{14}$$
$$\theta'' + \left(1 + \varphi'\right)^2\cos\theta\sin\theta + 3\sin^2\varphi\sin\theta\cos\theta = 0. \tag{15}$$

This system has three equilibrium points: the stable local vertical with $\varphi = \pm(2n+1)\frac{\pi}{2}$, $\theta = \pm n\pi$, the unstable local horizontal with $\varphi = \pm n\pi$, $\theta = \pm n\pi$, and the unstable orbit normal with $\varphi = \varphi^*$, $\theta = \pm(2n+1)\frac{\pi}{2}$, where n is any integer and φ^* is any constant [6,7]. Additionally, there exists a constant C of the TSS motion (i.e., $C' = 0$), when the tether length remains constant ($\ell' = 0$), given by [6]

$$C = \theta'^2 + \cos^2\theta\left(\varphi'^2 - 1 - 3\sin^2\varphi\right) + 4, \tag{16}$$

where $0 \le C \le 4$, with $C = 0$ and $C = 4$ at the local vertical and orbit normal equilibrium points, respectively.

2.1. Analysis of Three-Dimensional Motion

If $\theta_0 = \theta_0' = 0$ in Equations (14) and (15), the pitch motion of the TSS is described by

$$\varphi'' - 3\sin\varphi\cos\varphi = 0. \tag{17}$$

The phase portrait of Equation (17), depicted in Figure 2, shows that the pitch motion of the TSS in the station-keeping phase is similar to a simple pendulum, such that the vertical position is a center and the local horizontal corresponds to a saddle point.

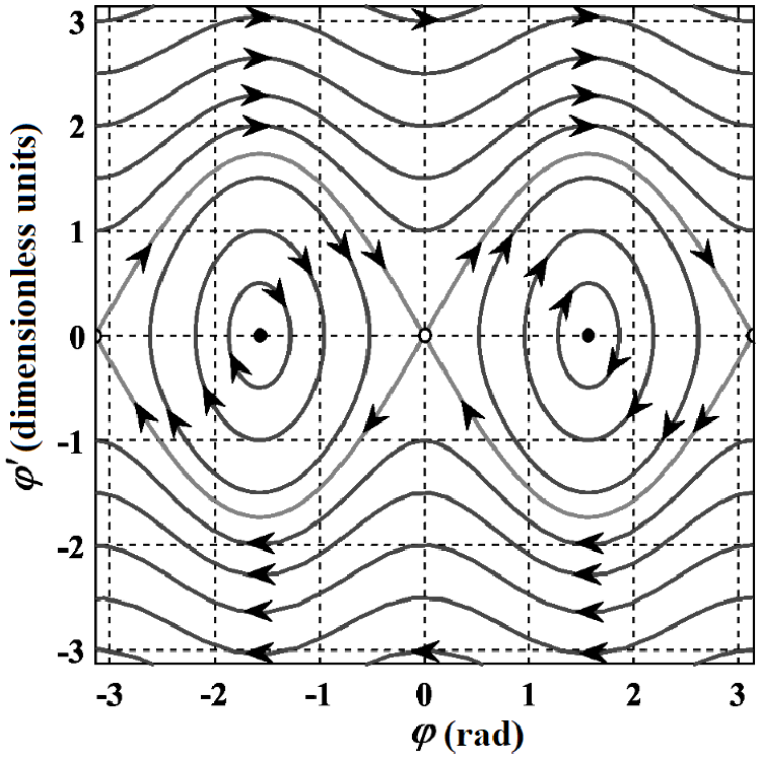

Figure 2. Pitch motion of the TSS in the station-keeping phase [39].

On the other hand, if $\theta_0 \neq 0$ or $\theta_0' \neq 0$ in Equations (14) and (15), quasi-periodic and chaotic motions can occur in the out-of-plane motion of the TSS [6,7]. For example, for a given value of C, Equations (14) and (15) are integrated numerically with $\varphi_0 = \varphi^*$, $\varphi_0' = 0$, $\theta = 0$, $\theta_0' = \sqrt{C - 4 + (1 + 3\sin^2\varphi^*)}$, for various values of φ^*, over 300 orbits. Note that the initial roll velocity is computed by using Equation (16). Then, the Poincaré map of the phase trajectories is taken as $\Sigma = \{(\varphi, \varphi')|\theta = 0, \theta' > 0\}$, sampled at period 2π. Figure 3 shows the Poincaré sections for $C = 2.5$, $C = 3.0$, $C = 3.25$, and $C = 3.75$, respectively. As can be seen from Figures 2 and 3, the periodic planar motion becomes quasi-periodic and chaotic. Similarly, Poincaré sections show that, if the local vertical ($\varphi_0 = \frac{\pi}{2}$, $\varphi_0' = 0$) is initially excited with $\theta_0 = 0$, $\theta_0' = \sqrt{C - 4 + (1 + 3\sin^2\frac{\pi}{2})} = \sqrt{C}$, then the stable equilibrium point turns into a quasi-periodic trajectory when $0 < C < 3.15$ but is replaced by a chaotic trajectory when $3.15 \leq C < 4$, as shown in Figure 4a,b. To study the control of the out-of-plane motion of TSS in this manner, the system is considered to begin at the local vertical position by applying the initial conditions $\varphi_0 = \frac{\pi}{2}$, $\theta_0 = 0$, $\varphi_0' = 0$, $\theta_0' = \sqrt{C}$, with $C = 3$ (quasi-periodic motion) and $C = 3.5$ (chaotic motion).

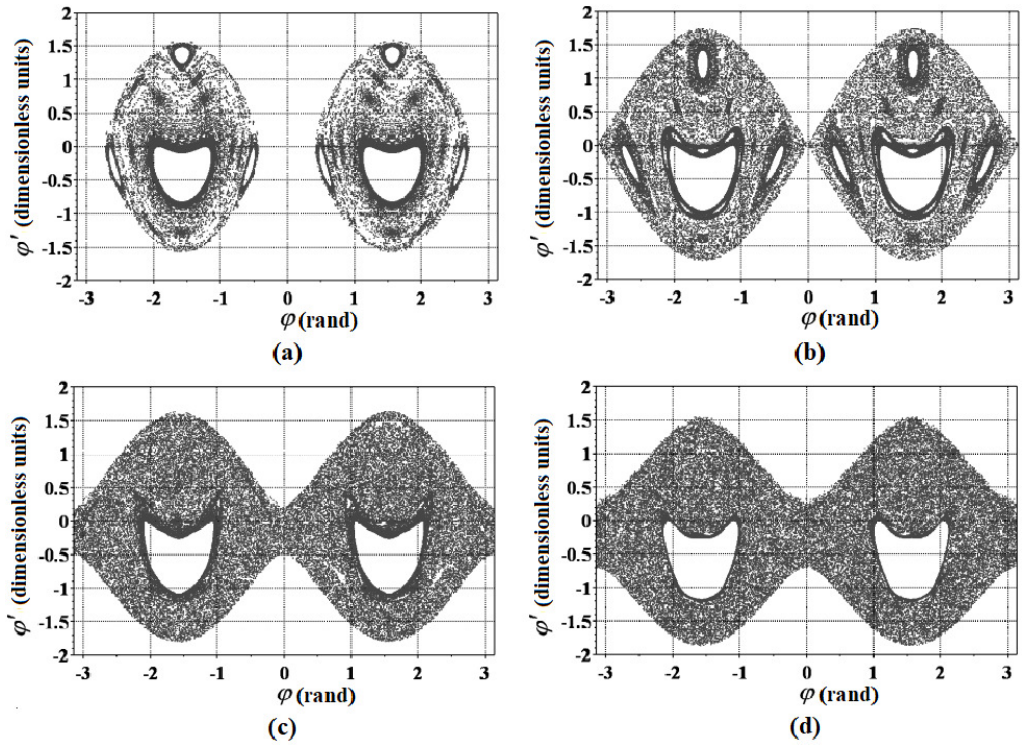

Figure 3. Poincaré sections for three-dimensional TSS motion for various $C > 0$. (**a**) $C = 2.5$, (**b**) $C = 3.0$, (**c**) $C = 3.25$, and (**d**) $C = 3.75$ are shown [39].

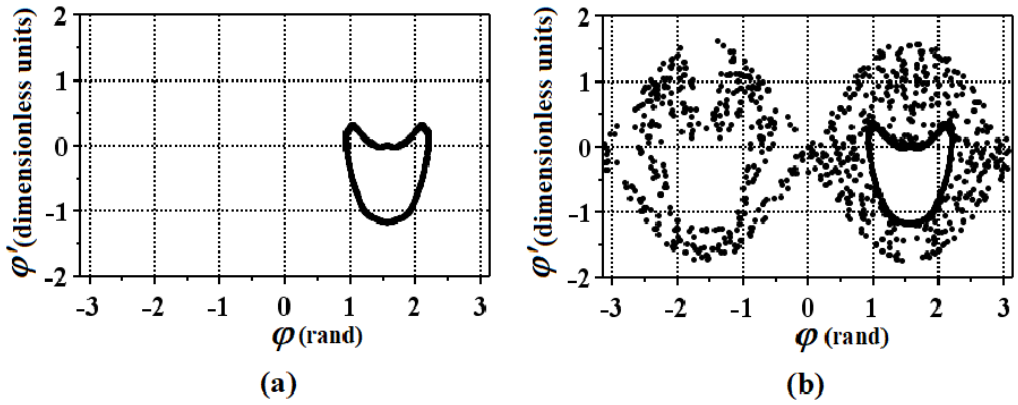

Figure 4. Poincaré sections for local vertical initially excited with $\theta_0' = \sqrt{C - 4 + (1 + 3\sin^2\frac{\pi}{2})}$. (**a**) $C = 3.14$ and (**b**) $C = 3.15$ are shown.

2.2. Tether Length Control

This section describes the Lyapunov function formulation (mission function) for controlling tether deployment/retrieval. The following positive definite function, which is related to the integral C, was selected as the trial Lyapunov function:

$$V = \frac{1}{2}\left[\rho'^2 + K_1\left(\rho - \rho_f\right)^2 + 3\rho^2 C^2\right], \tag{18}$$

where ρ_f is the desired final value of ρ; K_1 is a positive constant (non-dimensional gain); $V \geq 0$, and $V = 0$ if and only if at $\rho = \rho_f$, $\varphi = \pm(2n+1)\frac{\pi}{2}$, $\theta = \pm n\pi$, $\rho' = 0$, $\varphi' = 0$, $\theta' = 0$. The time derivative of V is given by

$$V' = \rho'\left[\rho'' + K_1\left(\rho - \rho_f\right) + 3\rho C\left(C - 4\left(\theta'^2 + \varphi'\cos^2\theta\left(1 + \varphi'\right)\right)\right)\right]. \tag{19}$$

Substituting Equation (11) into (19), we obtain

$$u = u_1 + u_2 + u_3, \tag{20}$$

where

$$u_1 = K_1\left(\rho - \rho_f\right) + K_2\rho', \tag{21a}$$

$$u_2 = \rho\left[\theta'^2 + \left(1+\varphi'\right)^2\cos^2\theta + \left(3\sin^2\varphi\cos^2\theta - 1\right)\right], \tag{21b}$$

$$u_3 = \rho\left[3C\left(C - 4\left(\theta'^2 + \varphi'\cos^2\theta\left(1+\varphi'\right)\right)\right)\right], \tag{21c}$$

as the nonlinear tension-control law, so that

$$V' = -K_2\rho'^2, \;\; K_2 > 0. \tag{22}$$

One can see from Equation (22) that $V' \leq 0$ with $V' = 0$ if and only if $\rho' = 0$. Thus, V' is negative semi-definite and the desired final state $\rho = \rho_f$, $\varphi = \frac{\pi}{2}$, $\theta = 0$, $\rho' = \varphi' = \theta' = 0$ is stable [42]. The limitation of this strategy is that we need a Lyapunov function to find the non-linear control. Actually, it can be derived only in simple cases, for example, when the system has an integral, as in this case. In this manner, linear approximations are much better and easier to implement.

In the next section, the TSS is assumed to be orbiting the Earth at an altitude of 220 km, with $\omega = 1.1804 \times 10^{-3}$ rad/s. The maximum tether length is assumed to be 1 km ($L = 1$ km), and the base satellite and subsatellite masses are set as $M = 1000$ kg and $m = 50$ kg.

3. Deployment and Retrieval Performances

The initial conditions for the tethered subsatellite motion are [25,29,38]:

$$\left(\rho_0, \rho_0', \varphi_0, \varphi_0', \theta_0, \theta_0'\right)^T = \left(0.01, 0.5, \frac{\pi}{2}, 0, 0, \sqrt{C}\right)^T,$$

where $C = 3.0$ and $C = 3.5$. The initial roll motion θ_0' was set so that quasi-periodic and chaotic solutions appear in the station-keeping phase, as shown in Figures 5a,b and 6a,b, respectively. Figures 5c and 6c show the Poincaré section obtained from these trajectories, indicating that quasi-periodicity and chaos do occur for $C = 3$ and $C = 3.5$, respectively.

The desired final conditions are $\left(\rho_f, \rho_f', \varphi_f, \varphi_f', \theta_f, \theta_f'\right)^T = \left(\rho_f^*, 0, \frac{\pi}{2}, 0, 0, 0\right)^T$, where $\rho_f^* = 1.0$ for deployment and $\rho_f^* = 0.01$ for retrieval. Based on the stability condition of the system, the gains selected are $K_1 = 2$, $K_2 = 6$ during deployment, and $K_1 = 1$, $K_2 = 6$ during retrieval. In this manner, the effect of the variable tether length on the three-dimensional solutions is computed by numerically solving Equations (11)–(13), and using the tension-control law u given by Equation (20). To confirm the feasibility of u, it must satisfy the necessary positiveness condition: $u \geq 0$, at any time.

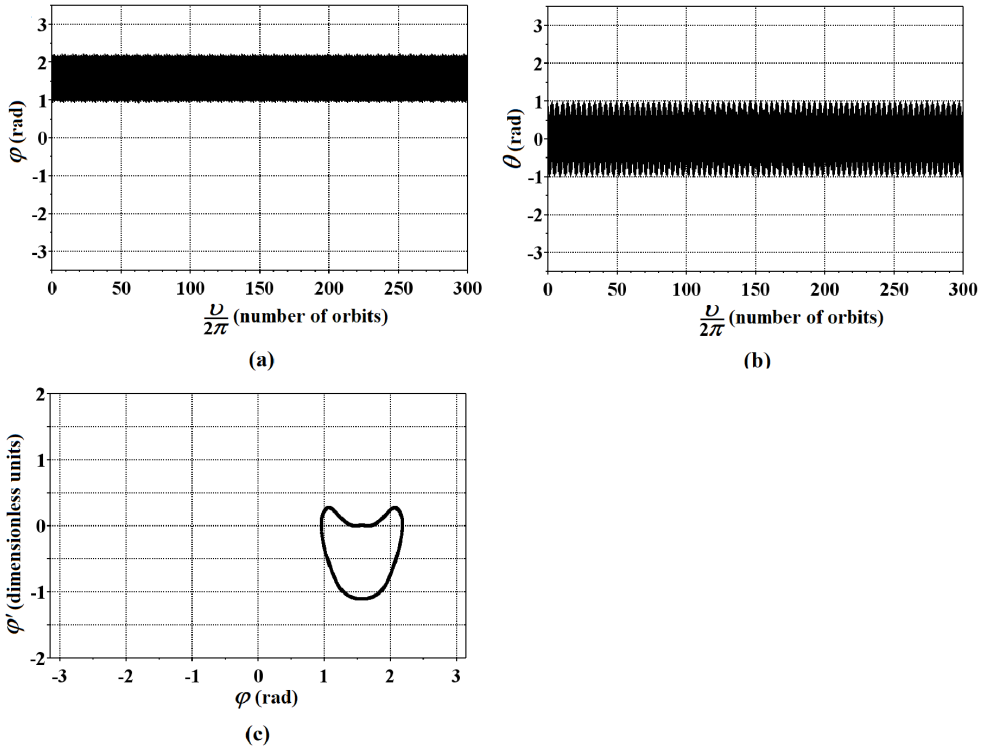

Figure 5. Quasi-periodic solution of the tethered subsatellite when the tether length remains constant. The system is considered to begin with the initial states $\left(\varphi_0, \varphi_0', \theta_0, \theta_0'\right)^T = \left(\frac{\pi}{2}, 0, 0, \sqrt{C}\right)^T$, where $C = 3$. (**a**,**b**) Pitch and roll angles versus true anomaly υ. (**c**) Poincaré section of the phase trajectories.

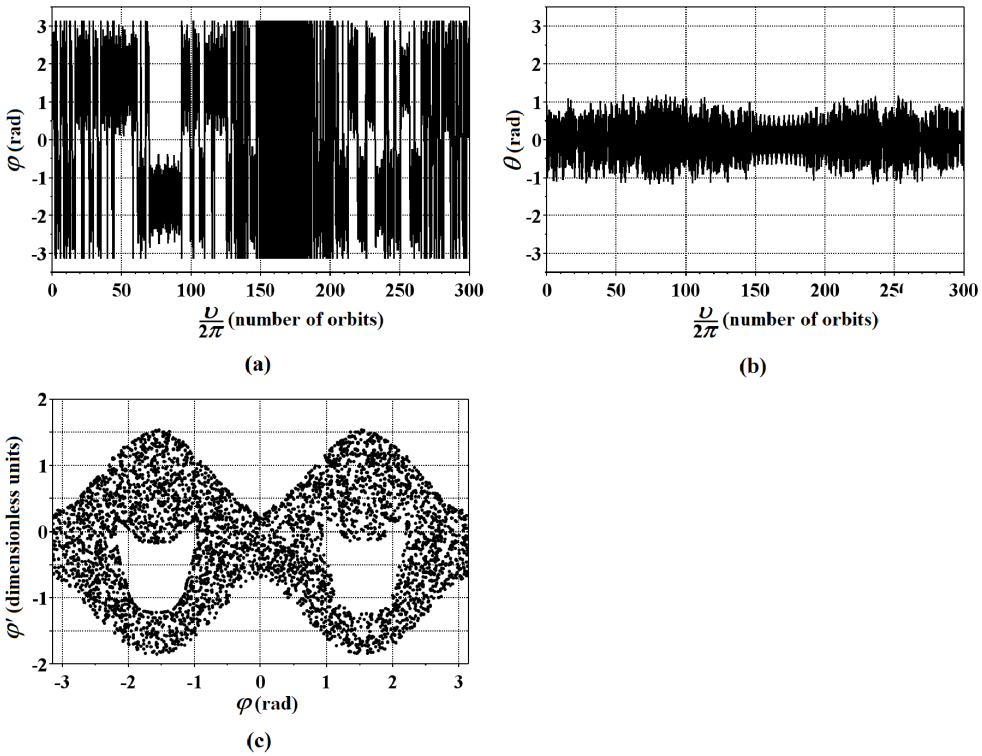

Figure 6. Chaotic solution of the tethered subsatellite when the tether length remains constant. The system is considered to begin with the initial states $\left(\varphi_0, \varphi_0', \theta_0, \theta_0'\right)^T = \left(\frac{\pi}{2}, 0, 0, \sqrt{C}\right)^T$, where $C = 3.5$. (**a**,**b**) Pitch and roll angles versus true anomaly υ. (**c**) Poincaré section of the phase trajectories.

Figures 7a,b and 8a,b show the effect of the variable length of the tether on the quasi-periodic and chaotic trajectories illustrated in Figures 5a,b and 6a,b, respectively. Figures 7a,b and 8a,b show the time history of the pitch and roll angles. Similarly, Figures 7c,d and 8c,d show the time history of the non-dimensional tether length and tension. The tension control (see Equation (20)) was always positive in both cases, and the deployment and retrieval phases were essentially complete in about five orbits. There exists a station-keeping phase when the deployment and retrieval phases are complete, as shown in Figures 7c,d and 8c,d. In the station-keeping phase, the tension control tends to stabilize about $u = 3$ ($\tau = 0.21$ N) when $\rho \approx 1$, and $u = 0$ when $\rho \approx 0.01$. Although the tension control performs well, and the tether achieves the desired final lengths, the pitch and roll angles oscillate about the equilibrium vertical position during the transfer from station-keeping to retrieval, as shown in Figures 7a,b and 8a,b. Note that the damping term in Equations (12) and (13) is proportional to ρ'. Thus, the pitch and roll motions are positively damped and stable during deployment but are negatively damped and unstable during retrieval, as shown in Figures 7a,b and 8a,b. However, as soon as the tension control caused the tether to retrieve from $\rho = 1$ to $\rho = 0.01$, the length rate settled down to $\rho' = 0$; the pitch motion returned to equilibrium; and the roll motion settled down to a sinusoidal oscillation of constant amplitude corresponding to a limit cycle [3]. In this connection, Banerjee and Kane [21], Xu et al. [44], Fujii and Ishijima [23], Kumar and Pradeep [30] proposed an out-of-plane thrusting for the retrieval phase to help stabilize this process.

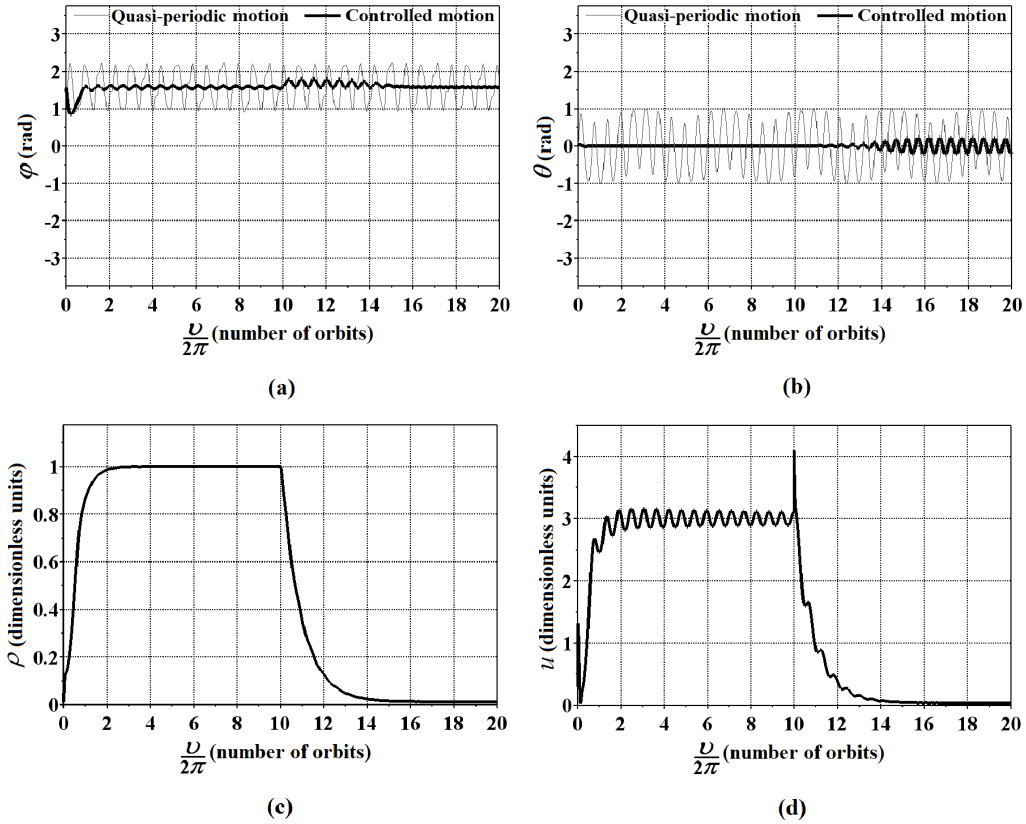

Figure 7. Controlled tether deployment and retrieval. (**a**,**b**) The effect of the variable length of the tether on the coupled pitch and roll motions when the system initiates with the quasi-periodic initial conditions described in Figure 5. (**c**,**d**) Non-dimensional tether length and tension.

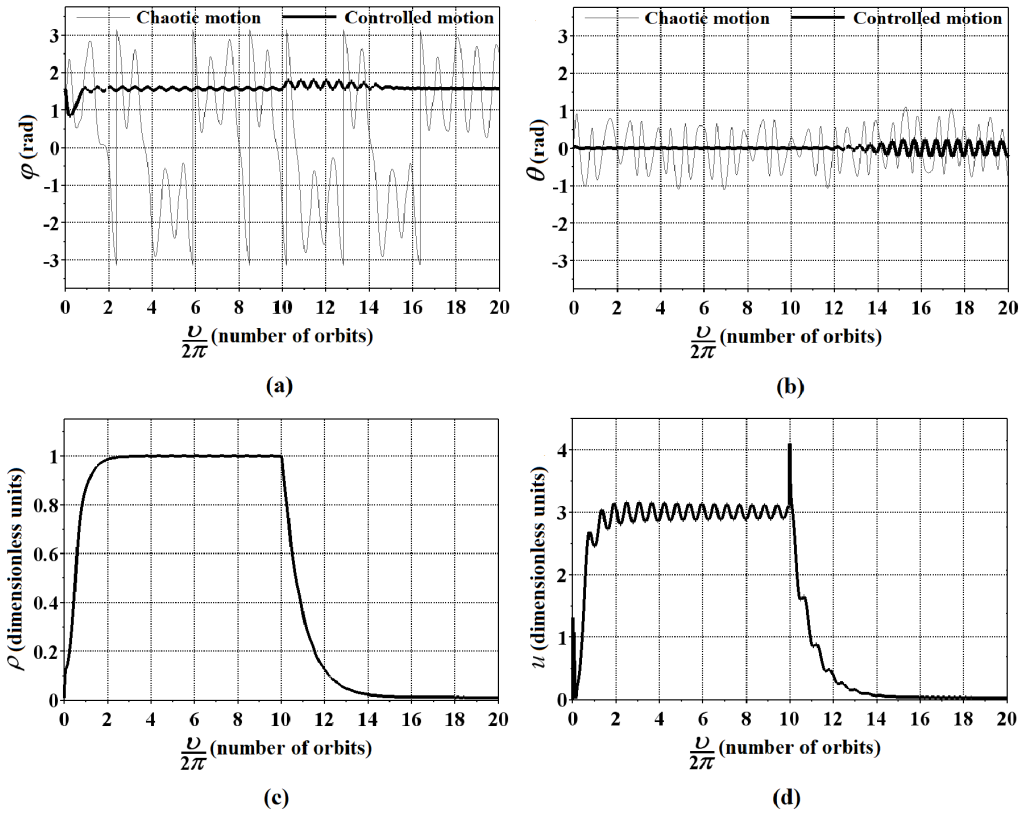

Figure 8. Controlled tether deployment and retrieval. (**a**,**b**) The effect of the variable length of the tether on the coupled pitch and roll motions when the system initiates with the chaotic initial conditions described in Figure 6. (**c**,**d**) Non-dimensional tether length and tension.

Figure 9 shows the in-plane and out-of-plane motion paths of the subsatellite for the controlled quasi-periodic (Figure 9a,b) and chaotic (Figuere 9c,d) trajectories. The right path in the in-plane motion corresponds to the deployment phase, and the left path, the retrieval phase. The station-keeping phase at the distance of $\ell = 1$ km and $\ell = 0.01$ km corresponds to the stationary points in the upper and lower parts, respectively. Although the retrieval phase is always unstable, the tension control (20) is very effective for controlling this system, which began with conditions that led to quasi-periodic and chaotic behavior in the station-keeping phase.

Finally, Figures 10 and 11 show the performance of a linear tension control implemented by Salazar and Prado [39] to suppress the chaotic behavior of a TSS on a deployment mission. The system initiates with conditions in such a way that we can obtain chaotic trajectories when the length of the tether is constant. Although the performance is similar to the non-linear tension control computed in this study, we noted that the initial pitch and tension oscillations were larger in the non-linear case. However, the linear-tension control used by Salazar and Prado [39] could not be used in retrieval missions because $\rho = 0$ creates a singularity in Equation (12), so the linearization could not be applied around the singularity $\rho = 0$.

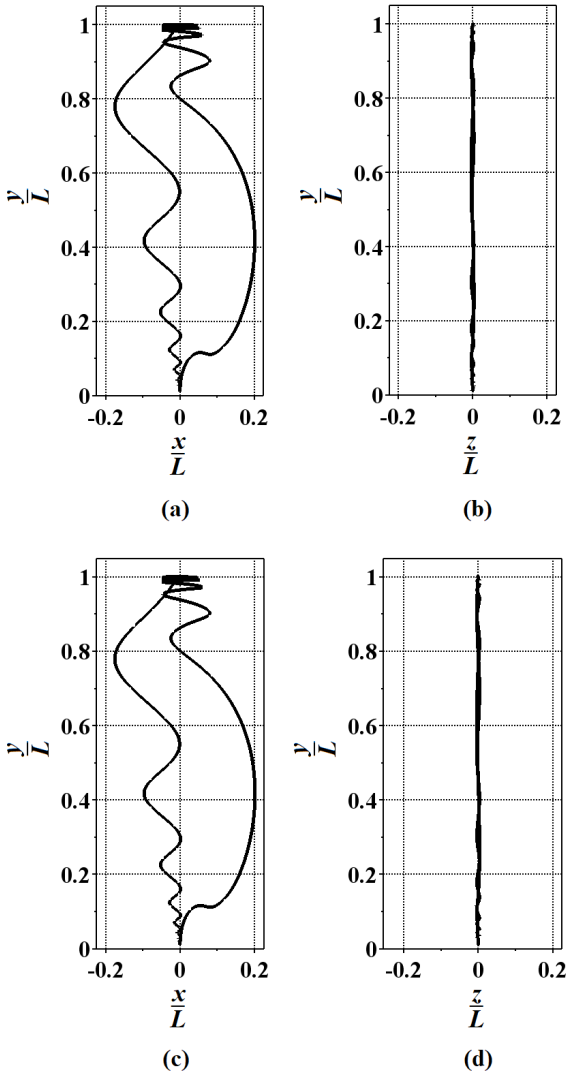

Figure 9. In-plane and out-of-plane motion paths of the subsatellite during the controlled deployment and retrieval. (**a**,**b**) Controlled quasi-periodic trajectory depicted in Figure 7. (**c**,**d**) Controlled chaotic trajectory depicted in Figure 8.

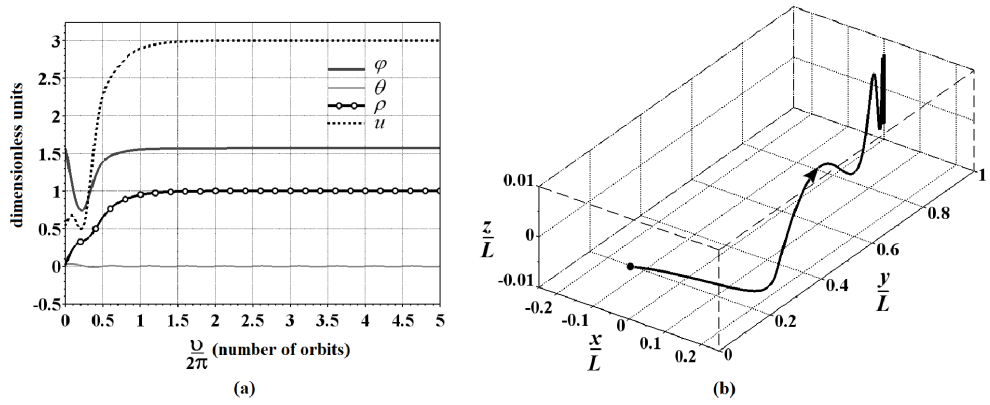

Figure 10. (**a**) Controlled Tether Deployment using a Linear Tension Control with the initial states $\left(\varphi_0, \varphi_0', \theta_0, \theta_0'\right)^T = \left(\frac{\pi}{2}, 0, 0, \sqrt{C}\right)^T$, where $C = 3.75$. (**b**) Three-dimensional motion path of the subsatellite during the controlled deployment [39].

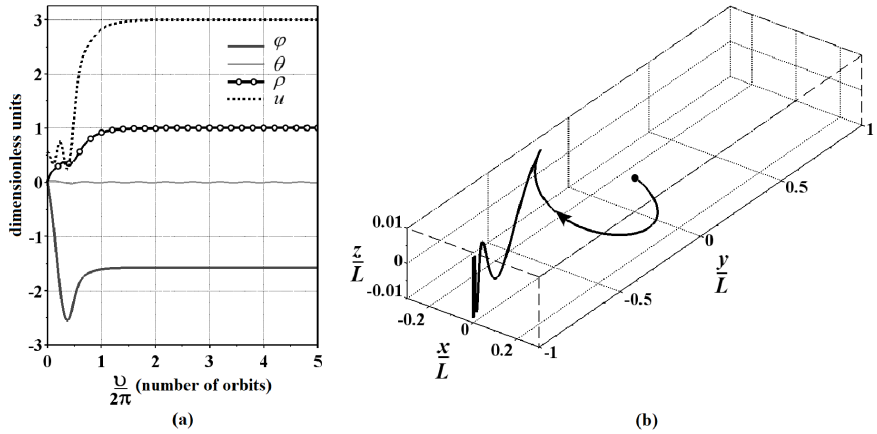

Figure 11. (**a**) Controlled tether deployment using a linear tTension control with the initial states $(\varphi_0, \varphi_0', \theta_0, \theta_0')^T = (0, 0, \frac{\pi}{30}, 0)^T$. (**b**) Three-dimensional motion path of the subsatellite during controlled deployment [39].

4. Conclusions

When the tether length remained constant, the stable local vertical position becames a quasi-periodic or chaotic trajectory if the out-of-plane motion was considered. In this study, a Lyapunov approach was used to determine a new nonlinear tension control law for controlling tether length. The importance of this study was to propose a non-linear tension control capable of guiding the chaotic subsatellite motion to the local vertical position by deployment/retrieval, whether or not chaos exists. This strategy can be applied in a tethered subsatellite orbiting the Earth in a Keplerian circular orbit, such that a constrained tension force is implemented on the tether during deployment and retrieval missions.

Considering the pitch and roll motions, the tethered subsatellite was deployed from a perturbed vertical position, such that quasi-periodicity and chaos occurred when the length of the tether was constant. The tension control was designed for deployment and retrieval missions, so the quasi-periodic and chaotic oscillations of the tether were suppressed. From the Lyapunov stability analysis performed about the local upward position, this final state was shown to be stable, but not asymptotically stable. Although a fast deployment/retrieval was accomplished by the nonlinear tension control law outlined in this paper, and the tension was capable of controlling the pitch-roll motion and guide the system to the desired final state, terminal small oscillations of the roll motion were seen during the retrieval phase. The result was a sinusoidal oscillation of constant amplitude about the final state. Thus, a new control law will be necessary to stabilize the pitch and roll angles at the local upward position when the length of tether is a maximum or minimum.

Author Contributions: Conceptualization, F.J.T.S. and A.B.A.P.; methodology, F.J.T.S. and A.B.A.P.; formal analysis, F.J.T.S.; investigation, F.J.T.S. and A.B.A.P.; writing—original draft preparation, F.J.T.S.; writing—review and editing, F.J.T.S. and A.B.A.P.; data curation, F.J.T.S.; formal analysis, F.J.T.S.; visualization, F.J.T.S. and A.B.A.P.; supervision, A.B.A.P.; project administration, A.B.A.P.; funding acquisition, A.B.A.P. All authors have read and agreed to the published version of the manuscript.

Funding: The authors would like to acknowledge their appreciation for the support from the Coordenacao de Aperfeicoamento de Pessoal de Nível Superior (Capes, Brasil), through grant #88887.478205/2020-00, for the support from the Fundacão de Amparo á Pesquisa do Estado de São Paulo (Fapesp, Brazil), through grant #2016/24561-0. This paper has been supported by the RUDN University Strategic Academic Leadership Program.

Institutional Review Board Statement: Not applicable.

Informed Consent Statement: Not applicable.

Data Availability Statement: The data presented in this study are available within the article.

Conflicts of Interest: The authors declare no conflict of interest.

References

1. Huang, P.; Zhang, F.; Chen, L.; Meng, Z.; Zhang, Y.; Liu, Z.; Hu, Y. A review of space tether in new applications. *Nonlinear Dyn.* **2018**, *94*, 1–19. [CrossRef]
2. Nixon, M.S.; Misra, A.K. Nonlinear dynamics and chaos of two-body tethered satellite systems. *Adv. Astronaut. Sci.* **1993**, *85*, 775–794.
3. Nixon, M.S. Nonlinear Dynamics and Chaos of Tethered Satellite Systems. Master's Thesis, McGill University, Montreal, QC, Canada, 1996.
4. Peng, J.H.; Liu, Y.Z. Chaotic motion of the tethered satellite system. *Tech. Mech.* **1996**, *16*, 327–331.
5. Steiner, W. Transient chaotic oscillations of a tethered satellite system. *Acta Mech.* **1998**, *127*, 155–163. [CrossRef]
6. Misra, A.K.; Nixon, M.S.; Modi, V.J. Nonlinear Dynamics of Two-Body Tethered Satellite Systems: Constant Length Case. *J. Astronaut. Sci.* **2001**, *49*, 219–236. [CrossRef]
7. Misra, A.K. Dynamics and control of tethered satellite systems. *Acta Astronaut.* **2008**, *63*, 1169–1177. [CrossRef]
8. Kojima, H.; Fukukawa, Y.; Trivailo, P.M. Experimental Verification of Periodic Libration of Tethered Satellite System in Elliptic Orbit. *J. Guid. Control Dyn.* **2011**, *34*, 614–618. [CrossRef]
9. Aslanov, V.S.; Ledkov, A.S. *Dynamics of Tethered Satellite Systems*, 1st ed.; Woodhead Publishing Limited: Sawston, UK, 2012.
10. Pang, Z.; Yu, B.; Jin, D. Chaotic motion analysis of a rigid spacecraft dragging a satellite by an elastic tether. *Acta Mech.* **2015**, *226*, 2761–2771. [CrossRef]
11. Aslanov, V.S. Chaos Behavior of Space Debris During Tethered Tow. *J. Guid. Control Dyn.* **2016**, *39*, 2399–2405. [CrossRef]
12. Yu, B.; Jin, D.; Wen, H. Nonlinear dynamics of flexible tethered satellite system subject to space environment. *Appl. Math. Mech.-Engl. Ed.* **2016**, *37*, 485–500. [CrossRef]
13. Aslanov, V.S.; Misra, A.K.; Yudintsev, V.V. Chaotic attitude motion of a low-thrust tug-debris tethered system in a Keplerian orbit. *Acta Astronaut.* **2017**, *139*, 419–427. [CrossRef]
14. Lian, X.B.; Liu, J.F.; Zhang, J.X.; Wang, C. Chaotic motion and control of a tethered-sailcraft system orbiting an asteroid. *Commun. Nonlinear Sci. Numer. Simul.* **2019**, *77*, 203–224. [CrossRef]
15. Yu, B.S.; Xu, S.D.; Jin, D.P. Chaos in a tethered satellite system induced by atmospheric drag and Earth's oblateness. *Nonlinear Dyn.* **2020**, *101*, 1233–1244. [CrossRef]
16. Modi, V.J.; Misra, A.K. On the deployment dynamics of tether connected two-body systems. *Acta Astronaut.* **1979**, *6*, 1183–1197. [CrossRef]
17. Chernous'ko, F.L. Dynamics of retrieval of a space tethered system. *J. Appl. Math. Mech.* **1995**, *59*, 165–173. [CrossRef]
18. Rupp, C.C. A tether tension control law for tethered subsatellites deployed along local vertical. In *NASA TMX-64963;* Marshall Space Hight Center: Huntsville, AL, USA, 1975.
19. Baker, P.W.; Dunkin, J.A.; Galaboff, Z.J.; Johnston, K.D.; Kissel, R.R.; Rheinfurth, M.H.; Siebel, M.P.L. Tethered Subsatellite Study. In *NASA TM X-73314;* Marshall Space Hight Center: Huntsville, AL, USA, 1976.
20. Bainum, P.M.; Kumar, V.K. Optimal-Control of the Shuttle-Tethered System. *Acta Astronaut.* **1980**, *7*, 1333–1348. [CrossRef]
21. Banerjee, A.K.; Kane, T.R. Tethered Satellite Retrieval with Thruster Augmented Control. *J. Guid. Control Dyn.* **1984**, *7*, 45–50. [CrossRef]
22. Misra, A.K.; Diamond, G.S. Dynamics of a subsatellite system supported by two tethers. *J. Guid. Control Dyn.* **1986**, *9*, 12–16. [CrossRef]
23. Fujii, H.; Ishijima, S. Mission function control for deployment and retrieval of a subsatellite. *J. Guid. Control Dyn.* **1989**, *12*, 243–247. [CrossRef]
24. Fujii, H.; Uchiyama, K.; Kokubun, K. Mission function control of tethered subsatellite deployment/retrieval: In-plane and Out-of-Plane Motion. *J. Guid. Control Dyn.* **1991**, *14*, 471–473. [CrossRef]
25. Vadali, S.R. Feedback tether deployment and retrieval. *J. Guid. Control Dyn.* **1991**, *14*, 469–470. [CrossRef]
26. Vadali, S.R.; Kim, E.S. Feedback control of tethered satellites using Lyapunov stability theory. *J. Guid. Control Dyn.* **1991**, *14*, 729–735. [CrossRef]
27. Fujii, H.A.; Anazawa, S. Deployment/retrieval control of tethered subsatellite through an optimal path. *J. Guid. Control Dyn.* **1994**, *17*, 1292–1298. [CrossRef]
28. Yu, S. On the dynamics and control of the relative motion between two spacecraft. *Acta Astronaut.* **1995**, *35*, 403–409. [CrossRef]
29. Pradeep, S. A new tension control law for deployment of tethered satellites. *Mech. Res. Commun.* **1997**, *24*, 247–254. [CrossRef]
30. Kumar, K.; Pradeep, S. Strategies for three dimensional deployment of tethered satellites. *Mech. Res. Commun.* **1998**, *25*, 543–550. [CrossRef]
31. Yu, S. Tethered Satellite System Analysis(1)—Two Dimensional Case and Regular Dynamics. *Acta Astronaut.* **2000**, *47*, 849–858. [CrossRef]
32. Barkow, B.; Steindl, A.; Troger, H.; Wiedermann, G. Various Methods of Controlling the Deployment of a Tethered Satellite. *J. Vib. Control* **2003**, *9*, 187–208. [CrossRef]
33. Steindl, A.; Troger, H. Optimal control of deployment of a tethered subsatellite. *Nonlinear Dyn.* **2003**, *31*, 257–274. [CrossRef]
34. Jin, D.P.; Hu, H.Y. Optimal Control of a Tethered Subsatellite of Three Degrees of Freedom. *Nonlinear Dyn.* **2006**, *46*, 161–178. [CrossRef]

35. Wen, H.; Jin, D.P.; Hu, H.Y. Optimal feedback control of the deployment of a tethered subsatellite subject to perturbations. *Nonlinear Dyn.* **2008**, *51*, 501–514. [CrossRef]
36. Wen, H.; Jin, D.; Hu, H. Three-dimensional optimal deployment of a tethered subsatellite with an elastic tether. *Int. J. Comput. Math.* **2008**, *85*, 915–923. [CrossRef]
37. Yu, B.S.; Jin, D.P. Deployment and retrieval of tethered satellite system under J2 perturbation and heating effect. *Acta Astronaut.* **2010**, *67*, 845–853. [CrossRef]
38. Sun, G.; Zhu, Z.H. Fractional-Order Tension Control Lawfor Deployment of Space Tether System. *J. Guid. Control Dyn.* **2014**, *37*, 2057–2062. [CrossRef]
39. Salazar, F.J.T.; Prado, A.F.B.A. Suppression of Chaotic Motion of Tethered Satellite Systems Using Tether Length Control. *J. Guid. Control Dyn.* **2021**, *45*, 580–586. [CrossRef]
40. Williams, P. A Review of Space Tether Technology. *Recent Patents Space Technol.* **2012**, *2*, 22–36. [CrossRef]
41. Misra, A.K.; Modi, V.J. Deployment and Retrieval of a Subsatellite Connected by a Tether to the Space Shuttle. *J. Guid. Control Dyn.* **1982**, *5*, 278–285. [CrossRef]
42. Wiggins, S. *Introduction to Applied Nonlinear Dynamical Systems and Chaos*, 2nd ed.; Springer: New York, NY, USA, 2003.
43. Jin, D.P.; Pang, Z.J.; Wen, H.; Yu, B.S. Chaotic motions of a tethered satellite system in circular orbit. *J. Phys. Conf. Ser.* **2016**, *744*, 012116. [CrossRef]
44. Xu, D.M.; Misra, A.K.; Modi, V.J. Thruster-Augmented Active Control of a Tethered Subsatellite System During its Retrieval. *J. Guid. Control Dyn.* **1986**, *9*, 663–672. [CrossRef]